Pergamon

Acta mater. Vol. 45, No. 8, pp. 3297–3310, 1997

Printed in Great Britain
PII: S1359-6454(97)00022-0
1359-6454/97 $17.00 + 0.00

DIFFUSION-CONTROLLED GRAIN GROWTH IN TWO-PHASE SOLIDS

DANAN FAN† and LONG-QING CHEN

Department of Materials Science and Engineering, The Pennsylvania State University, University Park, PA 16802, U.S.A.

(Received 29 May 1996; accepted 14 November 1996)

Abstract—Microstructural evolution and the kinetics of grain growth in volume-conserved two-phase solids were investigated using two-dimensional (2-D) computer simulations based on a diffuse-interface field model. In this model, a two-phase microstructure is described by non-conserved field variables which represent crystallographic orientations of grains in each phase and by a conserved composition field variable which distinguishes the compositional difference between the two phases. The temporal and spatial evolution of these field variables were obtained through a numerical solution to the time-dependent Ginzburg–Landau (TDGL) equations. The effect of the ratios of grain boundary energies to interfacial energy on the microstructure features was systematically studied. It was found that grain growth in a volume-conserved two-phase solid is controlled by long-range diffusion and follows the power growth law, $R^m - R_0^m = kt$ with $m = 3$ in the scaling regime for all cases studied, including the microstructures containing only quadrijunctions. The effects of volume fractions and initial microstructures are discussed.

1. INTRODUCTION

In two-phase ($\alpha + \beta$) polycrystalline solids, there are three kinds of interface: grain boundaries in α (α/α); grain boundaries in β (β/β); and interphase boundaries between α and β (α/β) (Fig. 1). If there are limited mutual solubilities between the two phases, grain growth through grain boundary migration and Ostwald ripening via long-range diffusion are expected to take place simultaneously during processing and service of these materials at high temperatures. Important practical examples include the ZrO_2–Al_2O_3 two-phase particulate composite in ceramics [1–3] and the two-phase ($\alpha + \beta$) titanium alloys in metallic systems [4, 5]. Even with the assumption of isotropic grain boundary energies and isotropic interphase boundary energy, theoretical treatment of microstructural coarsening in such systems is quite complicated because of the topological complexity and the fact that various diffusion paths are possible (Fig. 1). Most of the existing theoretical studies have been concentrated on grain growth in a single phase [6–9] or Ostwald ripening in a single crystal [10–13], or systems with small and immobile second-phase particles which cannot coarsen [14–16].

Recently, Cahn [17] performed a thermodynamic analysis for the stability of microstructures in a 2-D two-phase solid in which the volume fractions of the two phases are not conserved, i.e. the two phases have the same composition, and hence long-range diffusion and Ostwald ripening are not involved. In this theory, the microstructural stability and features were analyzed based on the energetic ratios of grain boundary energies to the interphase boundary energy, R_α and R_β: $R_\alpha = \gamma_\alpha/\gamma_{\alpha\beta}$, $R_\beta = \gamma_\beta/\gamma_{\alpha\beta}$, where γ_α is the grain boundary energy in α, γ_β is the grain boundary energy in β and $\gamma_{\alpha\beta}$ is the interphase boundary energy between α and β. These energetic ratios can be related to the dihedral angles as: $2\cos[\phi_\beta/2] = R_\alpha$ and $2\cos[\phi_\alpha/2] = R_\beta$, where ϕ_β is the dihedral angle formed by two α grains and a β grain, and ϕ_β is the angle formed by two β grains and an α grain. The relationship between microstructural stability and the energetic ratios is shown in Fig. 2. For $0 \leqslant R_\alpha \leqslant \sqrt{3}$, $\alpha\alpha\alpha$ trijunctions are stable, and when $R_\alpha > \sqrt{3}$, $\alpha\alpha\alpha$ trijunctions are unstable with respect to the nucleation of β grains. Similarly, $\beta\beta\beta$ trijunctions are stable for $0 \leqslant R_\beta \leqslant \sqrt{3}$ and are unstable with respect to the nucleation of α grains for $R_\beta > \sqrt{3}$; $\alpha\alpha\beta$ and $\alpha\beta\beta$ trijunctions are stable under the conditions of $0 \leqslant R_\alpha < 2$ and $0 \leqslant R_\beta < 2$, respectively. The quadrijunctions $\alpha\beta\alpha\beta$ will become stable for $R_\alpha^2 + R_\beta^2 \geqslant 4$.

Following Cahn's work, Holm *et al.* performed Monte Carlo simulations on the same system, i.e. a two-phase solid in which the volume fractions are not conserved [18]. They showed that microstructural features are indeed dependent on the energetic ratios (R_α and R_β) and quadrijunctions can be stable within a certain range of R_α and R_β as predicted by Cahn's

†Present address: Theoretical Division, MS B262, Los Alamos National Laboratory, Los Alamos, NM 87545, U.S.A.

thermodynamic analysis. More surprisingly, based on the Monte Carlo simulations, they predicted that the grain growth in a two-phase system with only quadrijunctions may be frozen [18]. However, a recent study showed that this might not be true [19].

While some common features may be found between conserved and nonconserved systems, significant differences exist. For example, if the grain boundary energy of one phase is lower than both the interphase boundary energy and the grain boundary energy of the other phase, the two-phase microstructure will evolve eventually to a single phase in a nonconserved system [18]. This is certainly not the case in a conserved system. Moreover, while the grain growth kinetics in a nonconserved two-phase system is similar to that in a single-phase system [18], grain growth in a conserved two-phase solid is likely to be controlled by long-range diffusion, i.e. similar to Ostwald ripening. It may be emphasized that essentially all two-phase solids of practical importance have the volume fractions of each phase conserved. Therefore, the focus of this paper will be on microstructural evolution in two-phase solids with the volume fractions conserved and with long-range diffusion.

Based on a diffuse-interface description [20], we recently developed a computer simulation model for studying the microstructural evolution in two-phase solids [21]. Earlier, a similar model has been applied to grain growth in single-phase systems [22–25]. One of the main advantages of this model is that any arbitrary microstructure can be easily treated since the interfaces are not singular surfaces requiring imposition of moving boundary conditions, but just a region where the fields have high gradients. For the special case of a circular grain, the boundary velocity obtained for the diffuse interface agrees very well with the analytical solution in the corresponding sharp-interface limit [26].

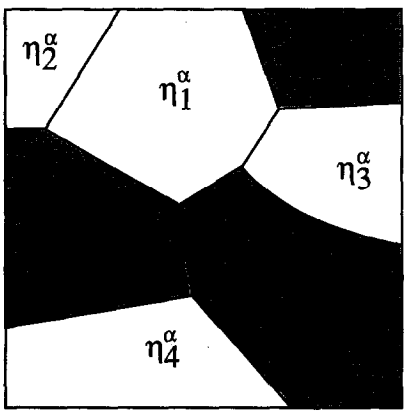

Fig. 1. Schematic description of a two-phase microstructure; η_i^α $(i = 1, \ldots, p)$ and η_j^β $(j = 1, \ldots, p)$ are orientation field variables with each orientation field representing grains of a given crystallographic orientation of a given phase (denoted as α and β with different compositions). Diffusion can occur along grain boundaries and interfaces as well as the crystalline lattice.

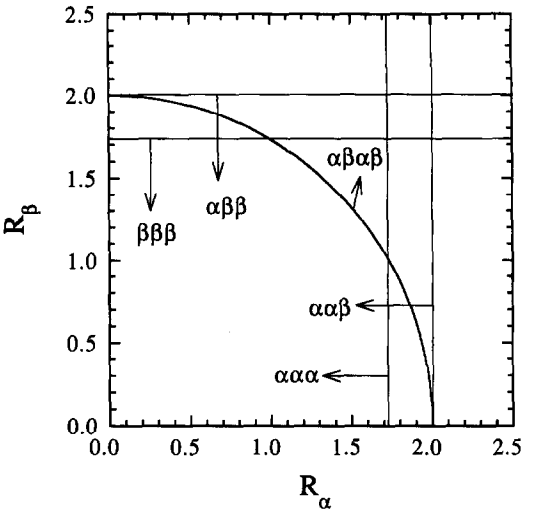

Fig. 2. Stability ranges of microstructural features in two phase systems. (Adapted from J. W. Cahn [17].)

The main purpose of this paper is to investigate the stability and scaling of two-phase microstructures, the grain size distributions, the grain growth kinetics, and the dependence of grain growth kinetics on the volume fractions as well as on the relative values of grain boundary energies and the interphase boundary energy. The topological evolution in a two-phase solid under various conditions will be discussed in a separate publication.

2. THE MODEL

2.1. Description of a two-phase microstructure

The details about this model have been discussed previously [21–25]. To describe an arbitrary two-phase polycrystalline microstructure (Fig. 1) using the diffuse-interface theory, a set of continuous field variables is defined in this model:

$$\eta_1^\alpha(r), \eta_2^\alpha(r), \ldots, \eta_p^\alpha(r), \eta_1^\beta(r), \eta_2^\beta(r), \ldots, \eta_q^\beta(r), C(r) \tag{1}$$

where η_i^α $(i = 1, \ldots, p)$ and η_j^β $(j = 1, \ldots, q)$ are called orientation field variables with each representing grains of a given crystallographic orientation of a given phase (denoted as α or β). The concept of the orientation field variables is similar to that of the different spins in the Monte Carlo Potts models for discretizing the orientation field. However, those field variables are continuous in space with assuming continuous values ranging from -1.0 to 1.0 in this model. For example, a value of 1.0 for $\eta_1^\alpha(r)$ with all other orientation variables 0.0 means that the material at position r belongs to an α-phase grain with the crystallographic orientation labeled as 1. At the grain boundary region between two α-grains with orientations 1 and 2, $\eta_1^\alpha(r)$ and $\eta_2^\alpha(r)$ will have absolute values intermediate between 0.0 and 1.0. Discretizing

the orientation field requires that all orientation variables have the equal possibility of formation, which is achieved in this model by constructing the proper free energy functional of a two-phase system (Section 2.3). In reality, the number of orientations in space is infinite. However, a large but finite number of orientation variables is enough to simulate the microstructural evolutions [21, 23]. $C(r)$ is the composition field which takes the value of C_α within an α grain and C_β within a β grain. $C(r)$ has intermediate values between C_α and C_β at the interfacial region between an α grain and a β grain. Therefore, with the set of field variables, we can completely describe a microstructure with α- and β-phase grains in different orientations, the α–α and β–β grain boundaries, and the α–β interphase boundaries (Fig. 1).

2.2. *Energetics of a two-phase system*

According to the diffuse-interface theories [20], the total free energy of a two-phase system, F, can be approximated as the sum of the free energy density and gradients of phase fields, i.e.

$$F = \int \Bigg[f_o(C(r); \eta_1^\alpha(r), \eta_2^\alpha(r), \ldots, \eta_p^\alpha(r); \eta_1^\beta(r), \eta_2^\beta(r), \ldots, \eta_q^\beta(r)) + \frac{\kappa_C}{2}(\nabla C(r))^2 + \sum_{i=1}^{p} \frac{\kappa_i^\alpha}{2}(\nabla \eta_i^\alpha(r))^2 + \sum_{i=1}^{q} \frac{\kappa_i^\beta}{2}(\nabla \eta_i^\beta(r))^2 \Bigg] \mathrm{d}^3 r \quad (2)$$

where f_o is the local free energy density, ∇C, $\nabla \eta_i^\alpha$ and $\nabla \eta_i^\beta$ are gradients of concentration and orientation fields, κ_C, κ_i^α and κ_i^β are the corresponding gradient energy coefficients, and p and q represent the number of field variables for the α and β phases. The coupling terms and higher order terms of field gradients have been ignored in the current model.

The energy of a planar grain boundary, σ_{gb}^α, between an α grain of orientation i and another α grain of orientation j may be calculated as follows:

$$\sigma_{gb}^\alpha = \int_{-\infty}^{+\infty} \left[\Delta f(\eta_i^\alpha, \eta_j^\alpha, C) + \frac{\kappa_C}{2}\left(\frac{\mathrm{d}C}{\mathrm{d}x}\right)^2 + \frac{\kappa_i^\alpha}{2}\left(\frac{\mathrm{d}\eta_i^\alpha}{\mathrm{d}x}\right)^2 + \frac{\kappa_j}{2}\left(\frac{\mathrm{d}\eta_j^\alpha}{\mathrm{d}x}\right)^2 \right] \mathrm{d}x \quad (3)$$

in which

$$\Delta f(\eta_i^\alpha, \eta_j^\alpha, C) = f_o(\eta_i^\alpha, \eta_j^\alpha, C) - f_o(\eta_{i,e}^\alpha, \eta_{j,e}^\alpha, C_\alpha) - (C - C_\alpha)\left(\frac{\partial f_o}{\partial C}\right)_{\eta_{i,e}^\alpha, \eta_{j,e}^\alpha, C_\alpha} \quad (4)$$

where $f_o(\eta_{i,e}^\alpha, \eta_{j,e}^\alpha, C_\alpha)$ represents the free energy density minimized with respect to η_i^α and η_j^α at the equilibrium composition of the α phase C_α. The definition of grain boundary energy [equation (3)] includes the concentration gradient and therefore automatically takes into account solute segregation to grain boundaries. The grain boundary energy between two β grains can be calculated from the same equations by replacing α with β. Similarly, the interphase boundary energy between an α grain with orientation i and a β grain with orientation j can be defined [21].

2.3. *Construction of the local free energy density function of a homogeneous phase*

In order to solve the kinetic equations, we need to construct the free energy functional, f_o. It should have the following characteristics: (a) if the values for all the orientation field variables are zero, the free energy describes the dependence of the free energy of the liquid phase on composition; (b) the free energy density as a function of composition in a given α-phase grain is obtained by minimizing the above free energy with respect to the orientation field variable corresponding to that grain, under the condition that all other orientation field variables are zero. The free energy density as a function of composition of a given β-phase grain may be obtained in a similar way. Therefore, all the phenomenological parameters in the free energy model, in principle, may be fixed using the information about the free energies of the liquid, solid α phase and solid β phase.

Another main requirement for f_o is that it has $2p$ degenerate minima, for α phase, with equal depth located at $(\eta_1^\alpha, \eta_2^\alpha, \ldots, \eta_p^\alpha) = (1, 0, \ldots, 0), \ldots, (0, 0, \ldots, 1), (-1, 0, \ldots, 0), \ldots, (0, 0, \ldots, -1)$ in p-dimension orientation space at the equilibrium concentration C_α, and has $2q$ degenerate minima located at $(\eta_1^\beta, \eta_2^\beta, \ldots, \eta_q^\beta) = (1, 0, \ldots, 0), \ldots, (0, 0, \ldots, 1), (-1, 0, \ldots, 0), \ldots, (0, 0, \ldots, -1)$ for β phase at C_β. This requirement ensures that each point in space can only belong to one orientation and all orientation variables have equal possibility of formation.

It should be emphasized that since we are not interested in phase transformations between α and β or between liquid and solids, and since we are only concerned with the case where the interphase and grain boundary energies are isotropic in this paper, the exact form of the free energy density function may not be very important in modeling microstructural evolution in a two-phase solid. The reason is that the driving force for grain growth is the total grain and interphase boundary energy. Other important parameters are the diffusion coefficients and boundary mobilities. In other words, we assume that the values of the grain and interphase boundary energies together with the kinetic coefficients completely control the kinetics of microstructural evolution,

irrespective of the exact form of the free energy density functional. Therefore, we assume the following relatively simple free energy density function for the purpose of studying coarsening in a two-phase solid:

$$f_0 = f(C) + \sum_{i=1}^{p} f(C, \eta_i^\alpha) + \sum_{i=1}^{q} f(C, \eta_i^\beta) + \sum_{k=\alpha}^{\beta} \sum_{i=1}^{p} \sum_{j=1}^{q} f(\eta_i^k, \eta_j^k) \quad (5)$$

in which

$$f(C) = -(A/2)(C - C_m)^2 + (B/4)(C - C_m)^4 + (D_\alpha/4)(C - C_\alpha)^4 - (D_\beta/4)(C - C_\alpha)^4$$

$$f(C, \eta_j^\alpha) = -(\gamma_\alpha/2)(C - C_\beta)^2(\eta_i^\alpha)^2 + (\delta_\alpha/4)(\eta_i^\alpha)^4$$

$$f(C, \eta_j^\beta) = -(\gamma_\beta/2)(C - C_\alpha)^2(\eta_i^\beta)^2 + (\delta_\beta/4)(\eta_i^\beta)^4$$

$$f(\eta_i^k, \eta_j^k) = (\epsilon_{ij}^{kk}/2)(\eta_i^k)^2(\eta_j^k)^2$$

where C_α and C_β are the equilibrium compositions of α and β phases, $C_m = (C_\alpha + C_\beta)/2$, and A, B, D_α, D_β, γ_α, γ_β, δ_α, δ_β and ϵ_{ij}^{kk} are phenomenological parameters. It should be pointed out, however, that if our emphasis is on the thermodynamics of solidification of a liquid or on the effect of anisotropic interfacial energy on microstructural evolution, proper coupling terms between field variables, as required by the crystalline symmetries, should be included.

2.4. *The kinetic equations*

By defining orientation and composition field variables, the kinetics of coupled grain growth can be described by its spatial and temporal evolution. In the present model, the evolution kinetics of these field variables are described by the time-dependent

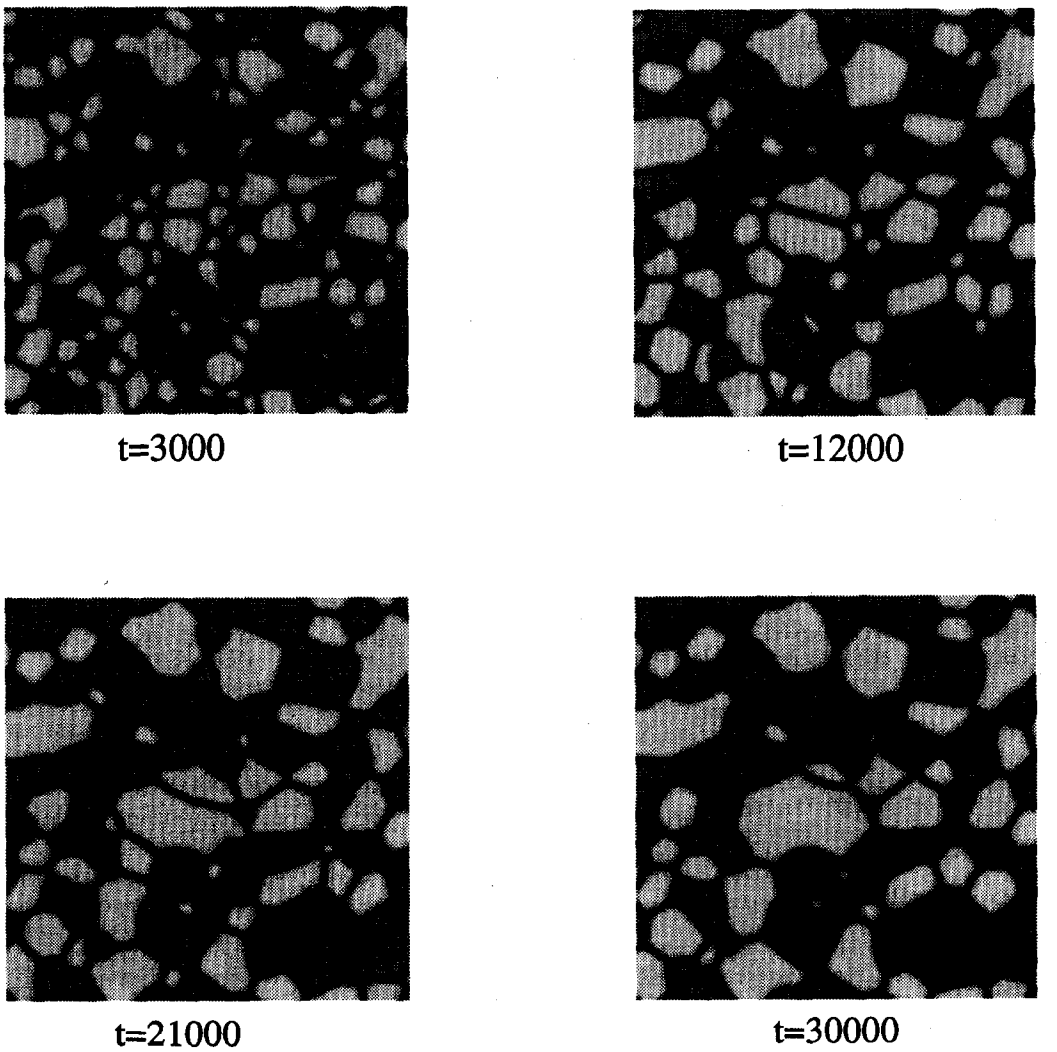

Fig. 3. Microstructural evolution in the system with $R_\alpha = R_\beta = 1.0$. The volume fraction of α phase is 50%. System size: 256 × 256. The initial structure is generated from a fine grain structure.

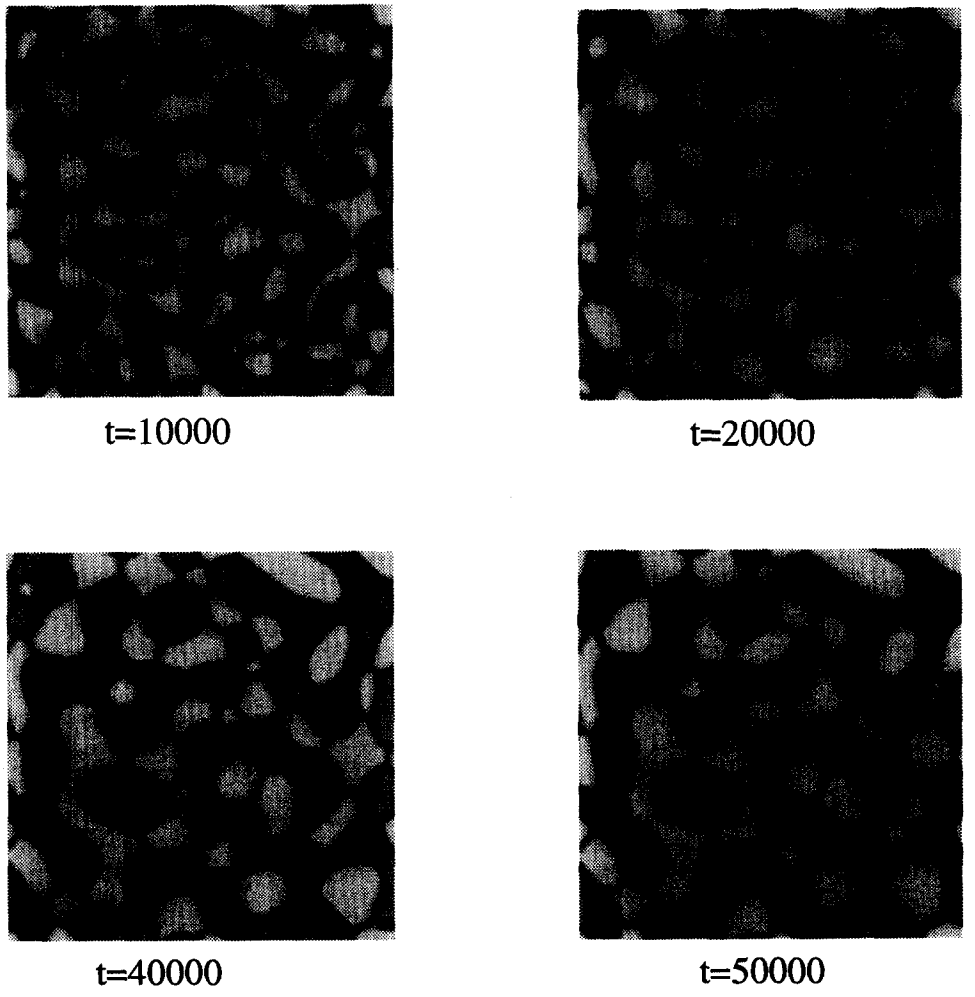

Fig. 4. Microstructural evolution in the system with $R_\alpha = R_\beta = 0.6$. The volume fraction of α phase is 50%. System size: 256 × 256. The initial structure is generated from a liquid.

Ginzburg–Landau (TDGL) [27] and Cahn–Hilliard [28] equations:

$$\frac{d\eta_i^\alpha(r,t)}{dt} = -L_i^\alpha \frac{\delta F}{\delta \eta_i^\alpha(r,t)}, \quad i = 1, 2, \ldots, p \quad (6a)$$

$$\frac{d\eta_i^\beta(r,t)}{dt} = -L_i^\beta \frac{\delta F}{\delta \eta_i^\beta(r,t)}, \quad i = 1, 2, \ldots, q \quad (6b)$$

$$\frac{dC(r,t)}{dt} = \nabla\left\{L_C \nabla\left[\frac{\delta F}{\delta C(r,t)}\right]\right\} \quad (6c)$$

where L_i^α, L_i^β and L_C are kinetic coefficients related to grain boundary mobilities and atomic diffusion coefficients, which may be functions of local orientation and composition field variables, t is time, and F is the total free energy given in equation (2). The difference between kinetic equations for orientation field variables $\eta_i^\alpha(r)$ or $\eta_i^\beta(r)$ and concentration field $C(r)$ comes from the fact that $C(r)$ is a conserved field, due to the requirement of mass conservation, whereas the orientation fields are nonconserved.

Once the free energy functional, f_o, is obtained, the gradient energy coefficients can be fitted to the grain boundary energies of the α and β phases, as well as the α/β interfacial energy. The kinetic coefficients, L_i^α, L_i^β and L_C, can be determined from grain boundary mobility and atomic diffusion data.

3. NUMERICAL SOLUTION

To numerically solve the set of kinetic equations (6), one needs to discretize them with respect to space. The Laplacian may be discretized by the following equation:

$$\nabla^2\phi = \frac{1}{(\Delta x)^2}\left[\frac{1}{2}\sum_j(\phi_j - \phi_i) + \frac{1}{4}\sum_{j'}(\phi_{j'} - \phi_i)\right] \quad (7)$$

where ϕ is any function, Δx is the grid size, j represents the set of first nearest neighbors of i, and j' is the set of second nearest neighbors of i. For discretization with respect to time, one may use the

following simple Euler technique:

$$\phi(t + \Delta t) = \phi(t) + \frac{d\phi}{dt} \times \Delta t \qquad (8)$$

where Δt is the time step for integration.

All the results discussed below were obtained by using the above discretization scheme and by assuming $\Delta x = 2.0$, $\Delta t = 0.1$. The kinetic equations are discretized using 256×256 or 512×512 points with periodic boundary conditions applied along both directions. The total number of orientation field variables for two phases is 30.

For starting a computer simulation, one may either input a pre-defined initial two-phase microstructure or generate the initial condition by assigning small random values to all the orientation field variables and the overall average composition to the composition variable at all positions, which simulates a liquid or disordered phase at a very high temperature. Because we can always normalize the length scale and time scale of kinetic equations (6) with diffusion coefficients and boundary mobilities, so we simply choose $L_\eta^\alpha = L_\eta^\beta = 1.0$ (isotropic grain η boundary mobility) and $L_C = 0.5$, which assumes the two phases have the same diffusion coefficients and boundary mobilities.

In this work, we assumed isotropic grain boundary energies for both phases and an isotropic interfacial energy between α and β phase, i.e. $\kappa_i^\alpha = \kappa_j^\alpha = \kappa^\alpha$ and $\kappa_i^\beta = \kappa_j^\beta = \kappa^\beta$. Furthermore, we assumed that the solubilities in the α and β phases are: $C_\alpha = 0.05$ and $C_\beta = 0.95$. The gradient energy coefficients and phenomenological parameters in the free energy function [equation (5)] are fitted to grain boundary energies, the interfacial energy, and their ratios. To get good statistics, all kinetic data and size distributions were obtained by employing 512×512 systems, in which there are more than 2700 grains initially and kinetic calculation is stopped at about 200 grains.

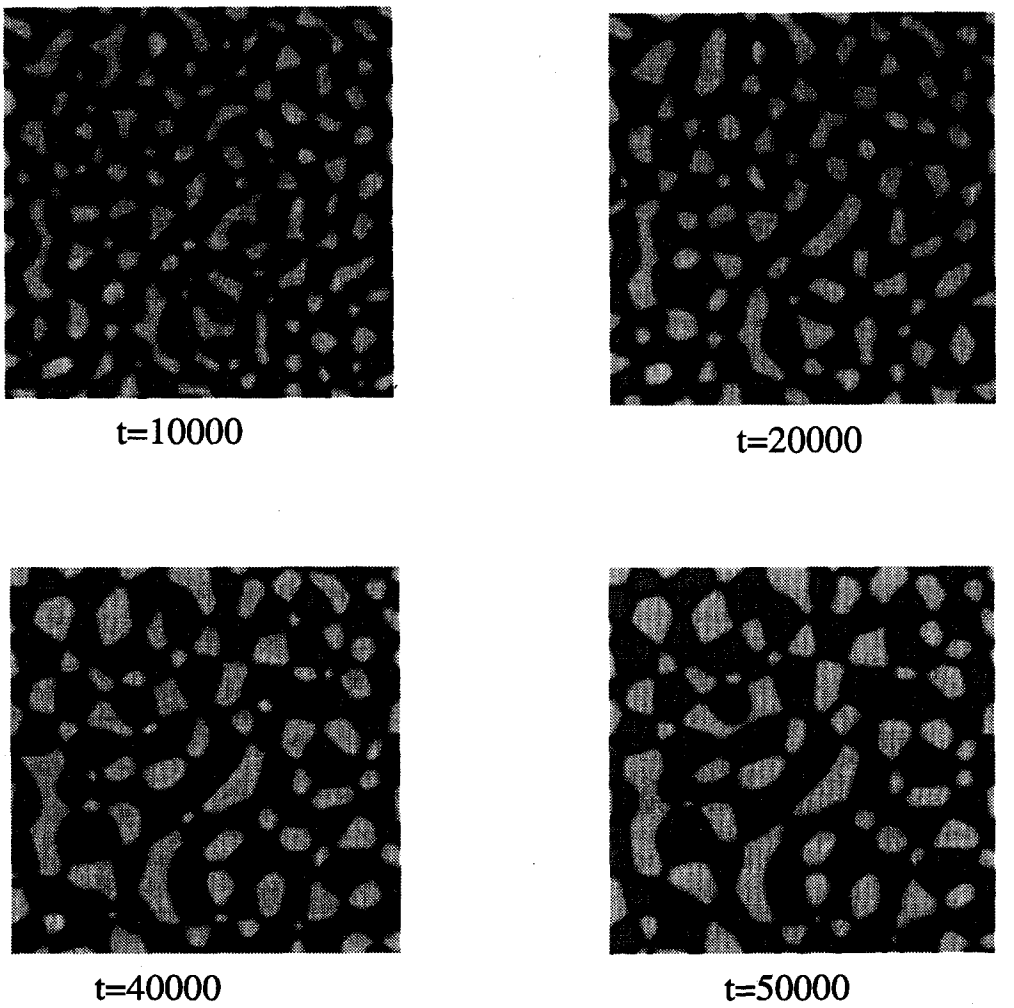

Fig. 5. Microstructural evolution in the system with $R_\alpha = R_\beta = 1.2$. The volume fraction of α phase is 50%. System size: 256×256. The initial structure is generated from a liquid.

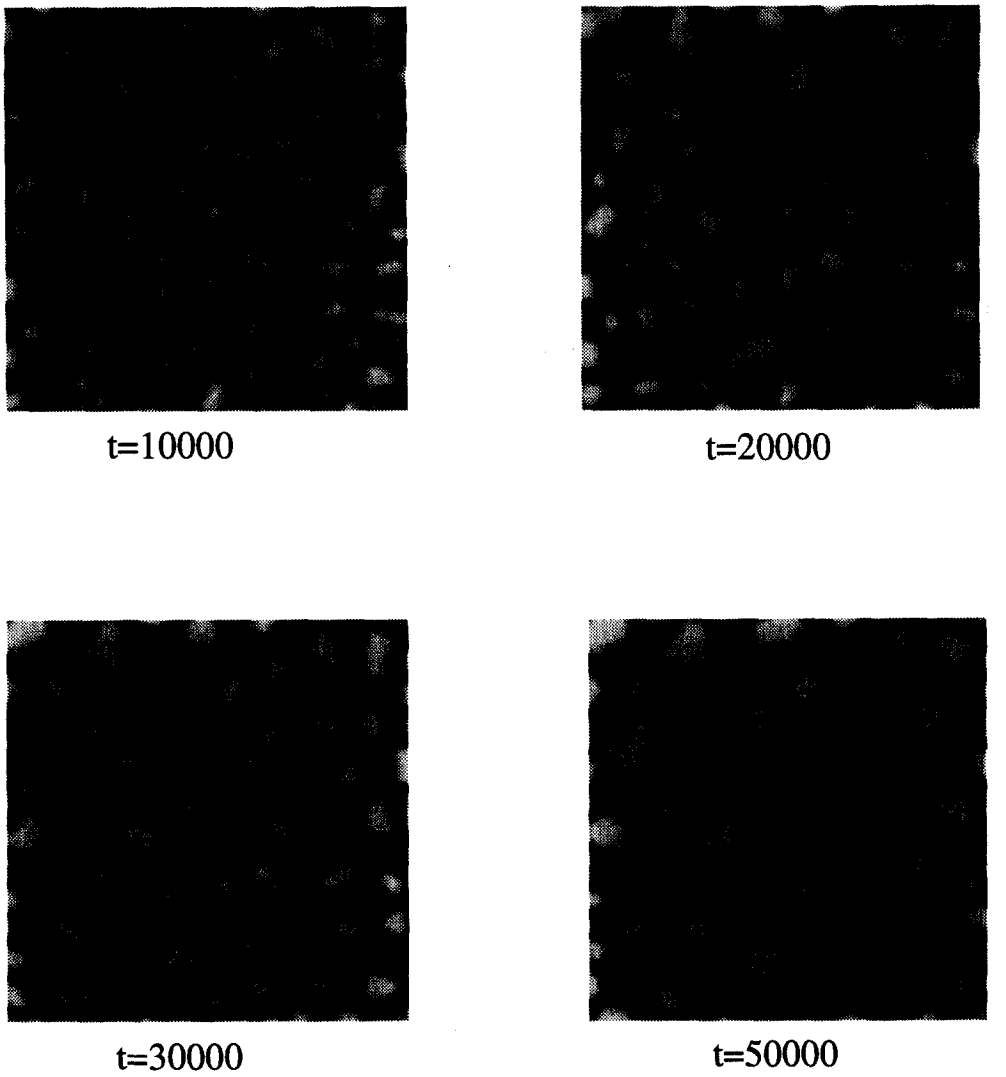

Fig. 6. Microstructural evolution in the system with $R_\alpha = R_\beta = 1.6$. The volume fraction of α phase is 50%. Both quadrijunctions and trijunctions are stable. System size: 256 × 256. The initial structure is generated from a liquid.

4. MICROSTRUCTURAL EVOLUTION

4.1. $R_\alpha = R_\beta$

In this section, we studied the case with 50% volume fraction of each phase and $R_\alpha = R_\beta$, i.e. the energetic ratios lie along the diagonal of the R_α–R_β plot in Fig. 2.

The simplest case is $R_\alpha = R_\beta = 1$, in which the interfacial energy between α and β is equal to the grain boundary energies in α and β. According to Cahn's analysis, in this case, $\alpha\alpha\alpha$, $\alpha\alpha\beta$, $\alpha\beta\beta$ and $\beta\beta\beta$ trijunctions are thermodynamically stable and equally favored. Here, $\alpha\alpha\alpha$ represents the trijunctions formed by three α grains and $\alpha\alpha\beta$ the trijunctions formed by two α grains and a β grain, and so on. The microstructural evolution in this system is shown in Fig. 3. It can be seen that the microstructures contain only trijunctions, consistent with the thermodynamic analysis [17]. During microstructural evolution, grain growth occurs in both phases. It is observed that the coarsening of a cluster of same-phase grains is relatively fast, whereas the growth and shrinkage of grains isolated by grains of the other phase is much slower, which is controlled by long-range diffusion.

Figure 4 is the corresponding microstructural evolution for $R_\alpha = R_\beta = 0.6$. In this system, all trijunctions are energetically stable and the interfacial energy $\gamma_{\alpha\beta}$ is larger than the grain boundary energies γ_α and γ_β. Therefore, the system tends to form as many grain boundaries as possible in order to minimize the total free energy of the system during coarsening. It can be seen that grains of the same phase evolve to form clusters to eliminate the α–β interfaces, and, as a result, grains of the same phase link together to maximize the grain boundary area and chain structures of grains of the same phase are formed.

If $R_\alpha = R_\beta > 1$, the system favors the formation of

α–β interfaces. Figure 5 is the microstructural evolution with $R_\alpha = R_\beta = 1.2$. In this system, instead of forming clusters of same-phase grains, there is a tendency to eliminate the grain boundaries due to their high energies. As a result, some elongated grains with more interfaces are formed during microstructural evolution as an attempt to reduce the total grain boundary area.

Microstructural evolution for $R_\alpha = R_\beta = 1.6$ is shown in Fig. 6. In this system, $1 < R_\alpha = R_\beta < \sqrt{3}$ and $R_\alpha^2 + R_\beta^2 = 5.12$, i.e. the condition $R_\alpha^2 + R_\beta^2 \geq 4$ for the stability of quadrijunctions is satisfied. Hence, both trijunctions and quadrijunctions $\alpha\beta\alpha\beta$ are energetically stable. It can be seen that a microstructure consists of trijunctions of $\alpha\alpha\beta$ or $\alpha\beta\beta$ and quadrijunctions $\alpha\beta\alpha\beta$, and the two phases are mutually dispersed to minimize the high-energy grain boundaries. Even though the trijunctions $\alpha\alpha\alpha$ and $\beta\beta\beta$ are still thermodynamically stable in this case, they are seldom observed. There are two reasons for this. First, grains of one phase tend to be surrounded by grains of the other phase in the initial grain structure formed by crystallization of a liquid. Secondly, trijunctions $\alpha\alpha\alpha$ and $\beta\beta\beta$ disappear more rapidly than $\alpha\alpha\beta$ and $\alpha\beta\beta$ because of high grain boundary energies and the fact that their disappearance is quite similar to grain growth in a single-phase solid.

In the system $\sqrt{3} < R_\alpha = R_\beta < 2$, trijunctions $\alpha\alpha\alpha$ and $\beta\beta\beta$ are thermodynamically unstable and the stable microstructure consists of only trijunctions $\alpha\alpha\beta$, $\alpha\beta\beta$ and quadrijunctions $\alpha\beta\alpha\beta$. The only difference between this system and the system with $R_\alpha = R_\beta = 1.6$ (Fig. 6) is the stability of trijunctions $\alpha\alpha\alpha$ and $\beta\beta\beta$. Since trijunctions $\alpha\alpha\alpha$ and $\beta\beta\beta$ are rarely observed in Fig. 6, microstructures obtained from this system are essentially similar to Fig. 6.

For the extreme condition, $R_\alpha > 2.0$ and $R_\beta > 2.0$,

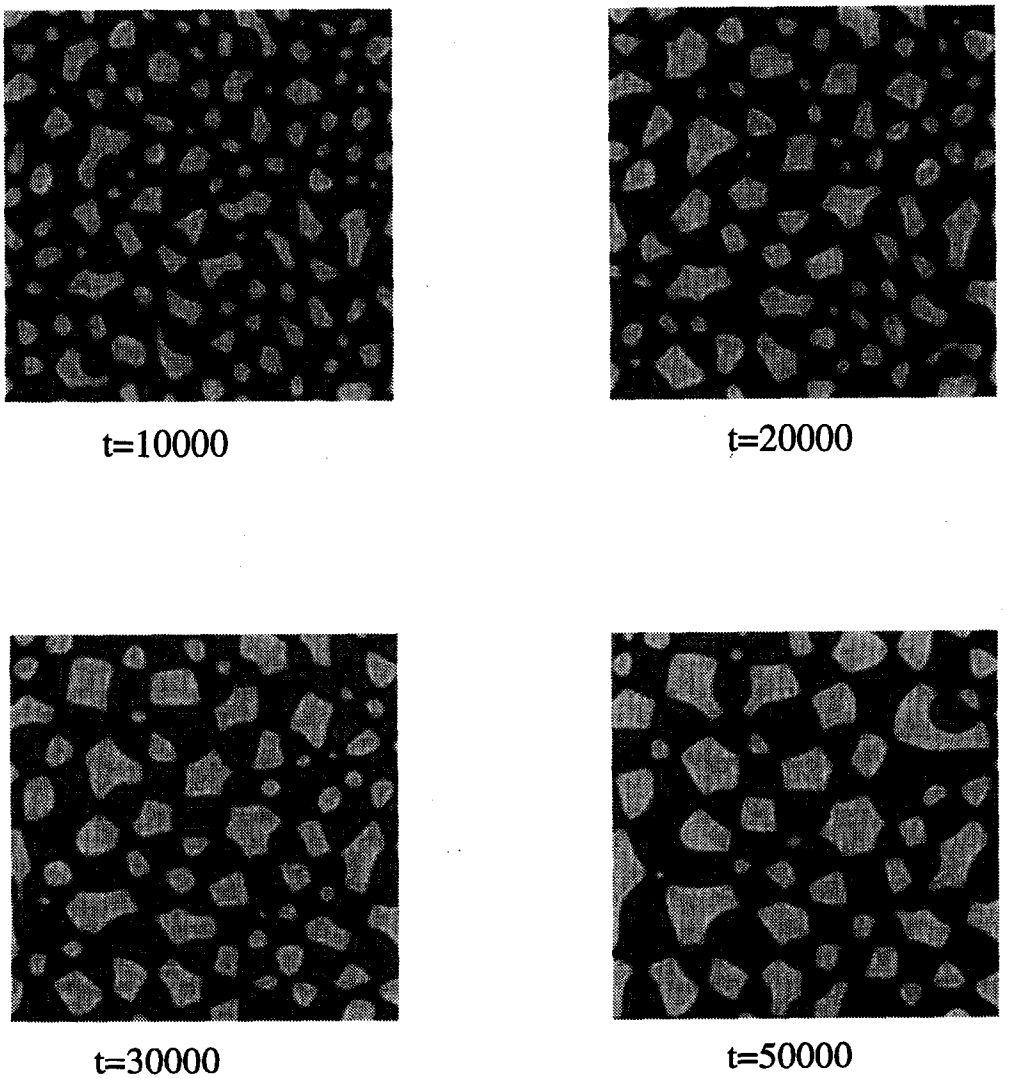

Fig. 7. Microstructural evolution in the system with $R_\alpha = R_\beta = 2.1$. The volume fraction of α phase is 50%. Only quadrijunctions are stable. System size: 256 × 256. The initial structure is generated from a liquid.

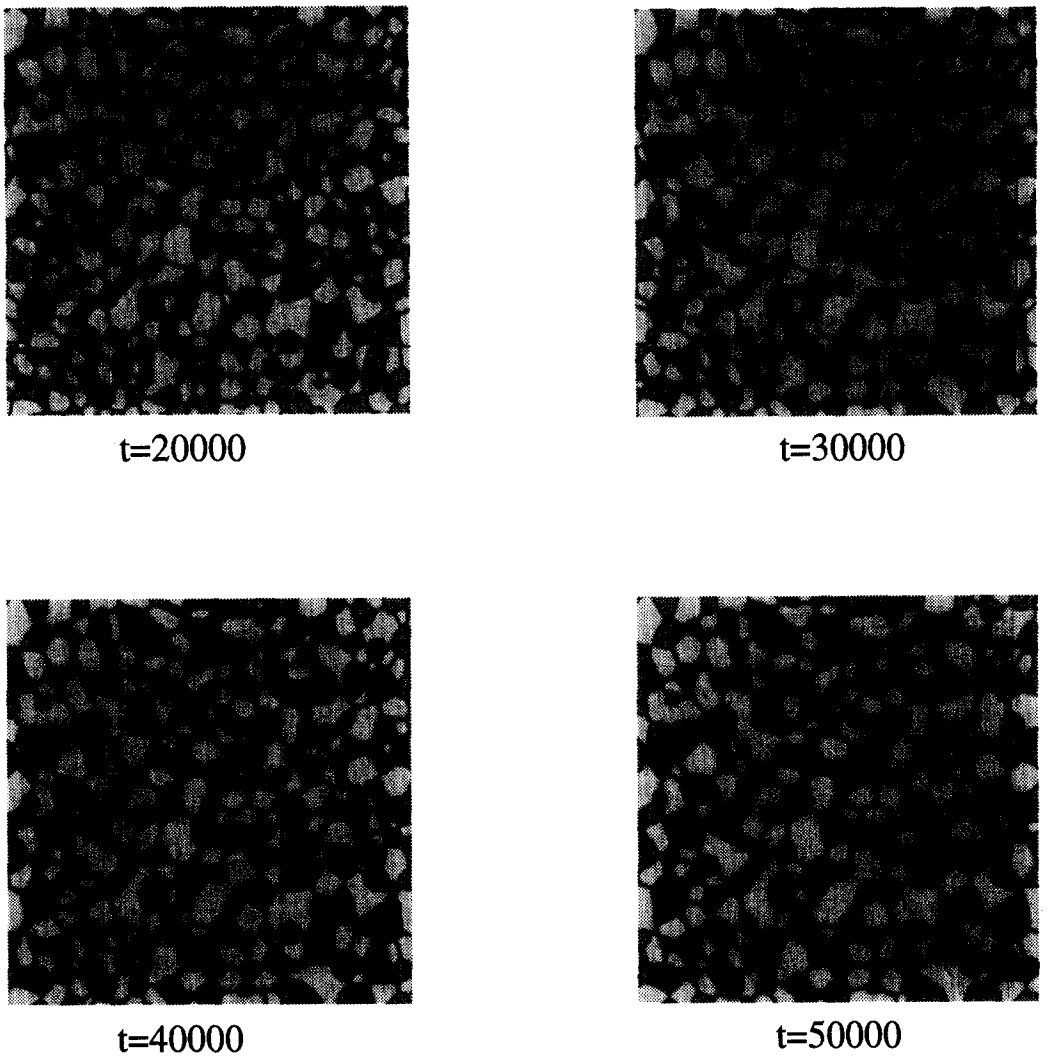

Fig. 8. Microstructural evolution in the system with $R_\alpha = 1.4$, $R_\beta = 0.97$. The volume fraction of α phase is 50%. The initial structure is generated from a fine grain structure. Al_2O_3 grains (α) are gray grains and ZrO_2 (β) are bright ones. System size: 512 × 512. The initial structure is generated from a fine grain structure.

so-called "double" wetting will occur. Under this condition, no trijunctions are stable and the only stable surfaces are the α β interfaces. The microstructural evolution for $R_\alpha = R_\beta = 2.1$ is shown in Fig. 7. The microstructures contain only quadrijunctions $\alpha\beta\alpha\beta$ and α–β interfaces. The angles of the quadrijunctions vary within a certain range, i.e. there is no thermodynamically fixed angle for quadrijunctions. The boundaries meeting at the quadrijunctions are not necessarily straight, which is assumed by the thermodynamic analysis [17]. Most of the interfaces are actually curved to fit into the quadrijunctions for the requirement of space filling and the balance of surface tensions which only require the tangents of those boundaries meeting at the quadrijunction balance each other.

4.2. $R_\alpha \neq R_\beta$

For $R_\alpha \neq R_\beta$, we consider a specific system, a Al_2O_3–ZrO_2 two-phase composite, as an example. It was reported [29] that the average ratio of grain boundary energy to interphase boundary energy in Al_2O_3 (denoted as α phase) is $R_\alpha = \sigma_{alu}/\sigma_{int} = 1.4$, and that in ZrO_2 (denoted as β phase) it is $R_\beta = \sigma_{zir}/\sigma_{int} = 0.97$. We ignore the anisotropy in the interphase and grain boundary energies. To generate the initial two-phase microstructure, a single-phase grain growth simulation was performed to obtain a fine grain structure. Grains are then randomly assigned with the equilibrium composition C_α or C_β and an orientation field, keeping the overall average composition corresponding to the desired equilibrium volume fractions. The purpose of generating the initial two-phase microstructure from a fine grain structure is to simulate the dense microstructures obtained from sintering of two-phase powders, as in Al_2O_3–ZrO_2.

The temporal microstructural evolution with 50%

Al_2O_3 (α phase) is shown in Fig. 8. In this system, $R_\alpha = 1.4 < \sqrt{3}$, $R_\beta = 0.97 < 1$ and $R_\alpha^2 + R_\beta^2 = 2.9 < 4$. Therefore, thermodynamically, all trijunctions are stable while no quadrijunctions are stable. These features can be clearly seen from Fig. 8. Furthermore, the microstructure evolves to eliminate the Al_2O_3 (α-phase) grain boundaries. This may be easily understood since the grain boundary energy in Al_2O_3 is much higher than both the grain boundary energy in ZrO_2 and the interphase boundary energy. As a result, Al_2O_3 grains (gray grains) tend to be isolated by ZrO_2 grains (bright grains).

It may be emphasized that, for $R_\alpha \neq R_\beta$, the microstructural stabilities in volume-conserved systems and nonconserved systems are quite different. According to Monte Carlo simulations [18], in a nonconserved system with $R_\alpha = 1.4$ and $R_\beta = 0.97$, only β phase is stable and only $\beta\beta\beta$ trijunctions exist since all α grains eventually disappeared due to their high grain boundary energy. However, this is clearly not the case in our volume-conserved system (Fig. 8).

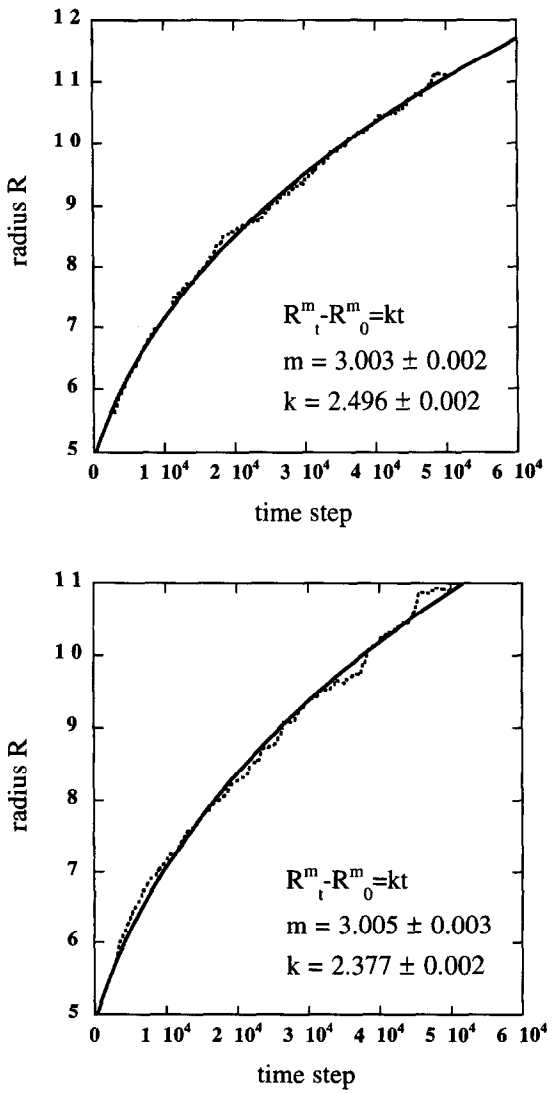

Fig. 9. Time dependence of the average grain size in the system $R_\alpha = R_\beta = 1.0$. The volume fraction of α phase is 50%; (a) α phase; (b) β phase.

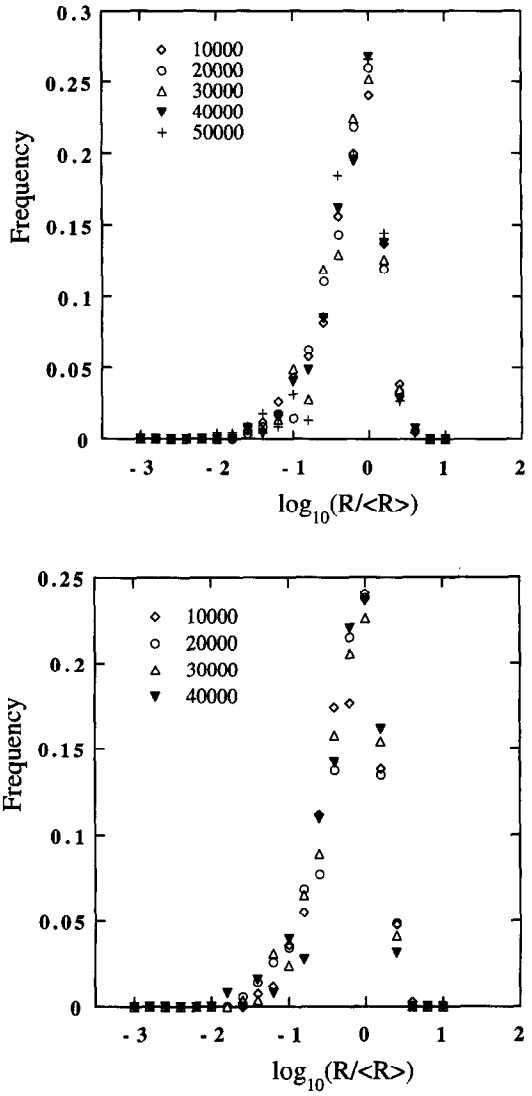

Fig. 10. Time dependence of the size distributions in the system $R_\alpha = R_\beta = 1.0$. The volume fraction of α phase is 50%; (a) α phase; (b) β phase.

5. COARSENING KINETICS AND SIZE DISTRIBUTIONS

5.1. Effect of the ratio of grain boundary energies and interphase boundary energy

Two cases, $R_\alpha = R_\beta = 1.0$ and $R_\alpha = R_\beta = 2.1$, are chosen to compare the effect of energetic conditions on the grain growth in two-phase solids. The time dependencies of the average grain size in α and β for $R_\alpha = R_\beta = 1.0$ are shown in Fig. 9(a) and (b), respectively. In these plots, the dotted lines are the data measured from the simulated microstructures and the solid lines are the non-linear fits to the power law $R_t^m - R_0^m = kt$. According to the non-linear fit, grain growth for both phases follows the power law with $m = 3$, a strong indication that the coupled grain

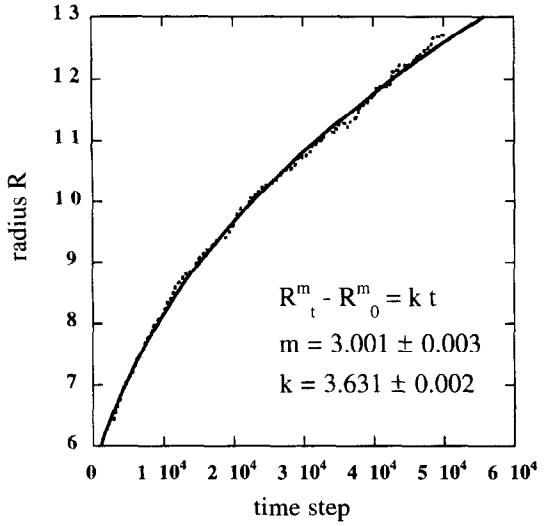

Fig. 11. Time dependence of the average grain size of the α phase in the system $R_\alpha = R_\beta = 2.05$. The volume fraction of α phase is 50%.

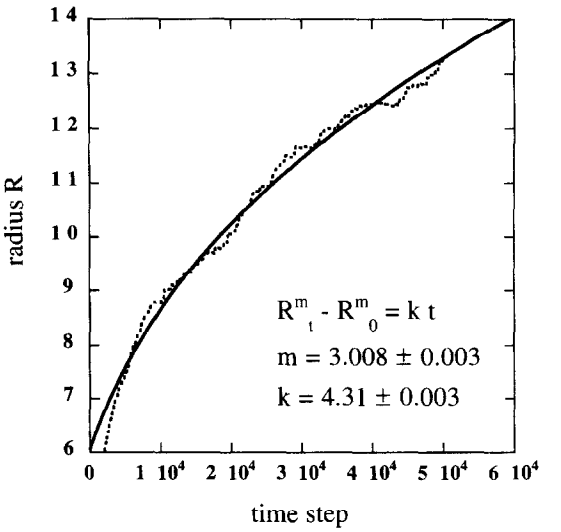

Fig. 13. Coarsening kinetics of the Al_2O_3 (α) phase in the system with $R_\alpha = 1.4$, $R_\beta = 0.97$. The volume fraction of α phase is 50%. The initial structure is generated from a fine grain structure.

growth is controlled by the long-range diffusion. It is not surprising that the kinetics coefficients k for the two phases are very similar since $R_\alpha = R_\beta$ and the volume fraction for each phase is 50%.

The corresponding grain size distributions for the system $R_\alpha = R_\beta = 1.0$ at several different time steps are shown in Fig. 10(a) and (b). It can be seen that distributions are asymmetric and the peaks of size distributions for both phases are centered around the average size [$\log_{10}(R/\langle R\rangle) = 0.0$] position. The shape of size distributions is independent of time for both phases, indicating that this system has reached the dynamic steady state or scaling after 5000 time steps. The size distributions are almost identical for the two phases.

For $R_\alpha = R_\beta = 2.1$, the time dependence of the average grain size in the α phase is shown in Fig. 11.

As discussed above, only quadrijunctions are stable in this system (Fig. 7). However, the grain growth still follows the power growth law with $m = 3$. Therefore, in contrast to the results from Monte Carlo simulations [18], quadrijunctions cannot stop the coupled grain growth in a two-phase solid. As a matter of fact, the coarsening of all quadrijunction microstructures is also controlled by the long-range diffusion in volume-conserved systems. It is noted that the kinetic coefficient k in this system is different from that for $R_\alpha = R_\beta = 1.0$. The only difference in these two systems is the energetic ratios or grain boundary energies and interfacial energy, which suggests that the kinetic coefficient k is dependent on the grain boundary energy and interfacial energies of a system.

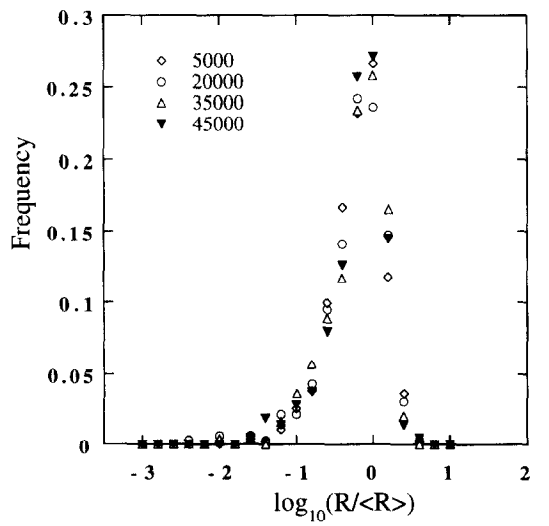

Fig. 12. Time dependence of the size distributions of the α phase in the system $R_\alpha = R_\beta = 2.05$. The volume fraction of α phase is 50%.

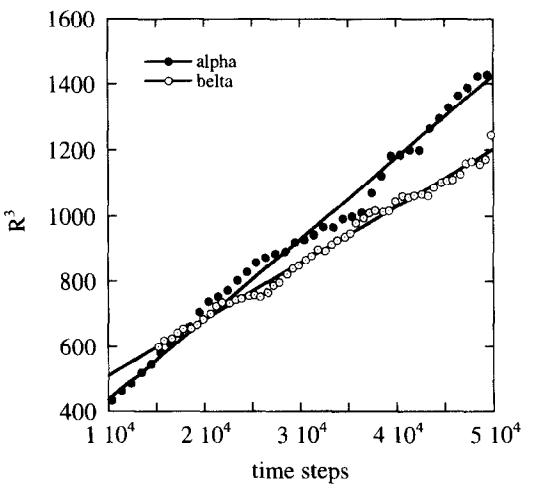

Fig. 14. Comparison of the coarsening kinetics of α and β phases in the system $R_\alpha = 1.4$, $R_\beta = 0.97$. The volume fraction of α phase is 50%. The initial structure is generated from a liquid.

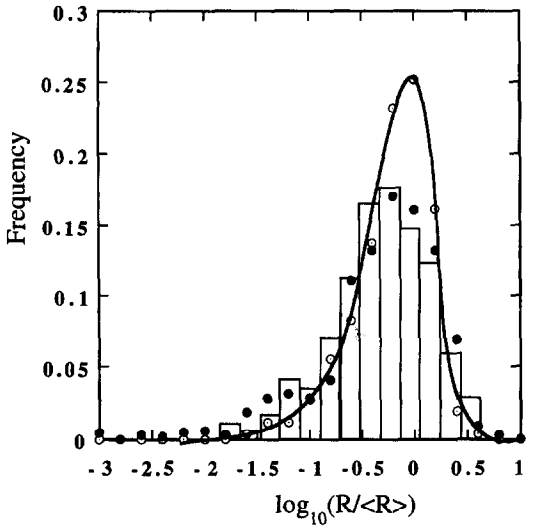

Fig. 15. Effect of initial microstructures on the size distributions of a phase in the system $R_\alpha = 1.4$, $R_\beta = 0.97$. The volume fraction of α phase is 50%. The solid line is the size distribution with initial structure generated from a liquid. The histogram is the size distribution with initial structure generated from a fine grain structure. Solid dots represent the distribution of the fine grain structure.

Figure 12 shows the time dependence of grain size distributions of the α phase for $R_\alpha = R_\beta = 2.1$. Similar to the case $R_\alpha = R_\beta = 1.0$, the scaling of microstructures is achieved, i.e. grain size distributions are time invariant. Both the growth exponent and the size distributions of the β phase are similar to those of the α phase. It is important to notice that the shapes of grain size distributions in these systems are similar to those for $R_\alpha = R_\beta = 1.0$. This observation may lead to a significant conclusion that, while the coarsening kinetics is dependent on the energetic conditions of a two-phase system, grain boundary energies and interfacial energies may not affect the grain size distributions during the steady state coarsening.

5.2. *Effect of initial microstructures*

We used two different ways to generate the initial microstructures: direct crystallization of both solid phases from a liquid and from a fine single-phase grain structure. We considered the case of $R_\alpha = 1.4$ and $R_\beta = 0.97$. The time dependence of the average grain size with 50% α phase and with the initial microstructure generated from a fine grain structure is shown in Fig. 13. Grain growth also follows the power law with $m = 3$ and $k = 4.31$ for α phase. Since $R_\alpha \neq R_\beta$, it is expected that the coarsening kinetics in two phases will not be the same. Indeed, in the β phase, the average grain size increases with time following the power law with $m = 3$ and $k = 3.8$.

Figure 14 is a comparison of coarsening kinetics in α and β with the initial microstructure generated from a liquid. To clarify the difference, R^3 is plotted against time steps. Under this initial condition, the coefficient k is 2.51 for the α phase and 1.99 for the β phase, which are about two times smaller than those obtained with the initial microstructure generated from a fine grain structure (Fig. 13). The reason for the slowdown is that, when the initial two-phase structure is generated from the solidification of an initially unstable liquid, grains of the α and β phases are alternatively distributed, i.e. each α grain having β grains as nearest neighbors and vice versa. While the initial microstructure is generated from a fine grain structure, clusters of same-phase grains exist (Fig. 8) in which grain growth is much faster, which in turn results in a larger kinetic coefficient.

The effect of the initial microstructure on the grain size distribution is compared in Fig. 15. In this plot, the solid line is a typical size distribution with the initial microstructure generated from a liquid, the histogram is the size distribution with the initial structure created from a fine grain structure, and the solid dots represent the size distribution of the initial fine grain structure. It can be seen that size distributions from different initial microstructures are quite different. The size distribution of the initial structure generated from a liquid (solid line in Fig. 15) is similar to those for $R_\alpha = R_\beta$ (Figs 10 and 11) whose initial microstructures were also generated from a liquid, indicating that energetic ratios do not affect the characteristics of the size distribution. On the other hand, the size distribution with the initial microstructure generated from a fine grain structure is almost identical to the original distribution of that fine grain structure. Therefore, in two-phase grain growth, size distributions are dependent on the initial microstructures and there is no unique size distribution for a given volume fraction and energetic ratios.

5.3. *Effect of volume fractions*

The effect of volume fractions is studied by comparing the grain growth in a system with 90% Al_2O_3 and that with 50% Al_2O_3. For both cases, the initial microstructures were generated from a fine grain structure. The microstructural evolution for 90% Al_2O_3 is shown in Fig. 16. The basic microstructural features are similar to those for 50% (Fig. 12) except that $\beta\beta\beta$ trijunctions do not exist due to the small volume fraction of the β phase. The effect of volume fractions on the coarsening kinetics is compared in Fig. 17, in which R^3 is plotted against t. The kinetic coefficient k for the α phase is 31.85 and 0.785 for the β phase. It can be seen that the variation of volume fractions will dramatically change the coarsening kinetics of both phases. The kinetic coefficient k for 90% α phase is about a magnitude larger than that of the 50% α-phase system ($k = 4.31$), while the k value is reduced about 5 times for the 10% β phase. As a result, the difference in k values for α and β phases is about 50 times. This dramatic variation comes from the different diffusion distances of the two phases during coarsening as the volume fraction changes. For the low-volume-fraction β

phase, the coarsening kinetics is solely controlled by Ostwald ripening and the typical diffusion distance is about the typical separation distance between β-phase grains. However, coarsening for the high volume fraction of α depends on the fraction of grain boundaries that are pinned by β grains and therefore the volume fraction of β. The influence of volume fractions on the grain size distributions is shown in Fig. 18. It can be seen that size distributions for both phases become more peaked than the original distribution of the initial fine grain structure and are also more peaked than that of the 50% α phase system with the same initial microstructure (Fig. 15). Therefore, the size distributions in the steady state may also vary as the volume fraction changes. However, in all circumstances, the mechanism of coarsening is still controlled by long-range diffusion and the coarsening kinetics follows the power growth law with $m = 3$, which is not affected by the energetic ratios, initial microstructures and volume fractions.

6. SUMMARY

The microstructural evolutions in volume-conserved two-phase solids were investigated by employing a diffuse-interface field model, in which the complexity of microstructural topology and long-range diffusion are automatically taken into account. It is shown that the stabilities of microstructural features in volume-conserved two-phase systems are mainly dependent on the ratios of grain boundary energies to interfacial energy, and the observed features are in agreement with previous thermodynamic analyses. The coupled grain growth in volume-conserved two-phase systems is controlled by long-range diffusion and follows the power growth law with $m = 3$, which is independent of the energetic ratios, initial microstructures and volume fractions, in contrast to the nonconserved systems in which $m = 2$. A two-phase microstructure containing only quadrijunctions can be stable under certain wetting conditions and it will coarsen according to the power law with $m = 3$, contrary to previous Monte Carlo

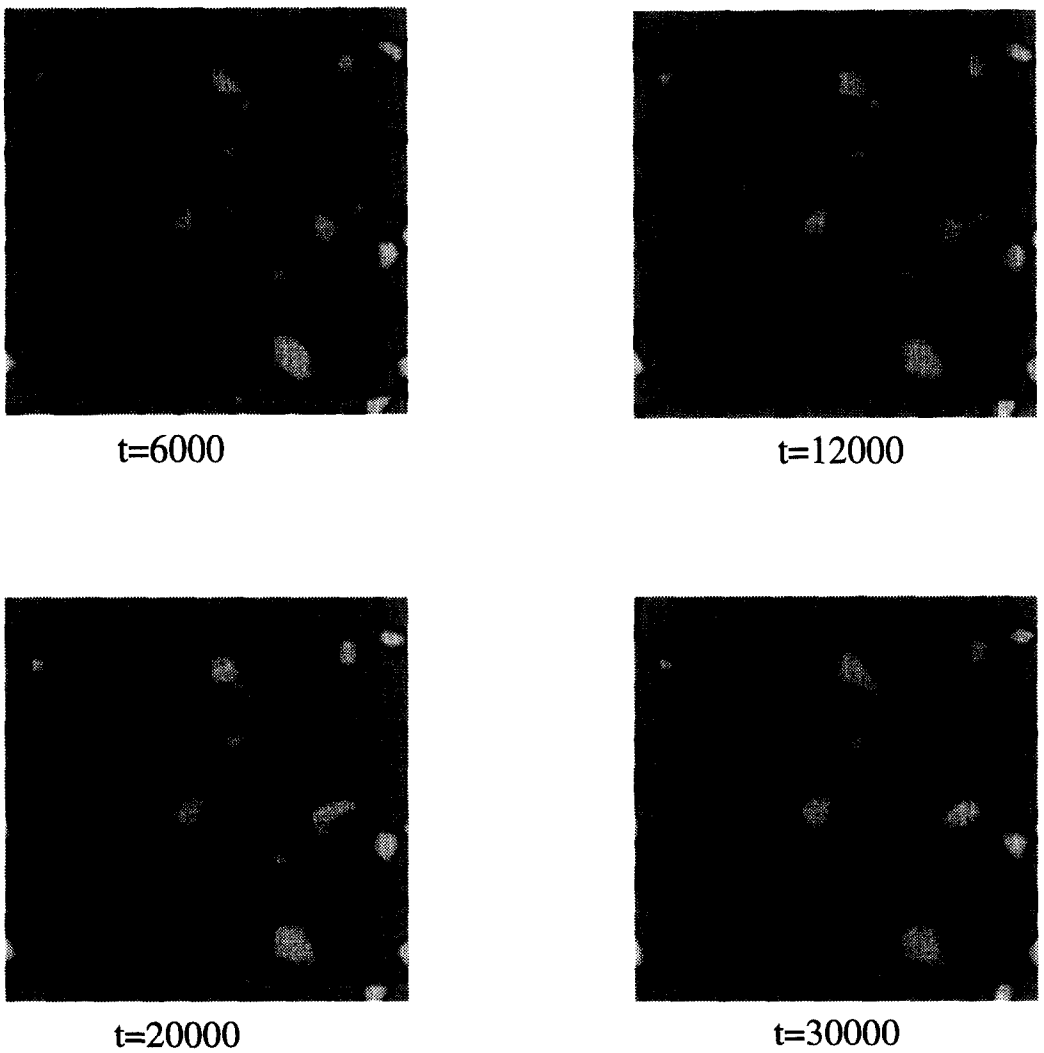

Fig. 16. Microstructural evolution in the system with $R_\alpha = 1.4$, $R_\beta = 0.97$. The volume fraction of β phase is 10%. System size: 256 × 256. The initial structure is generated from a fine grain structure.

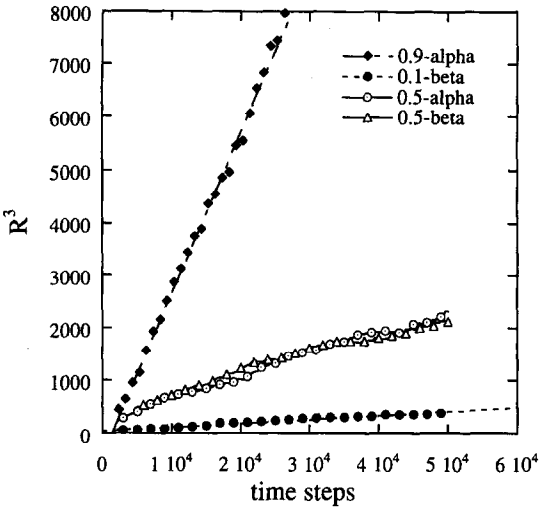

Fig. 17. Effect of volume fractions on the coarsening kinetics in the Al_2O_3 (α)–ZrO_2 (β) system. The volume fractions of ZrO_2 (β) phase are 10% and 50%. $R_\alpha = 1.4$, $R_\beta = 0.97$.

simulations. The kinetic coefficient k depends on the grain boundary energies, interfacial energy, initial microstructures and volume fractions. Among these factors, volume fractions of two phases have the most significant effect on the kinetic coefficient. In this study, we assumed a constant temperature. Of course, the kinetic coefficient k will be strongly dependent on the change in temperature. The scaling of grain size distributions is observed in all circumstances, i.e. they are time-invariant in the steady state. The characteristics of size distributions are independent of the energetic ratios of two-phase systems. However, they vary with the initial microstructures and the volume fractions. In this paper, the grain boundary mobilities and diffusivities for the two phases were assumed to be the same. Moreover, we did not separate the contributions from the grain boundary diffusion and lattice diffusion even though the effective lattice and grain boundary diffusivities can be derived from the kinetic equations. The effect of different diffusivities in the two phases and different diffusion paths on the grain growth in a two-phase solid will be investigated in the near future.

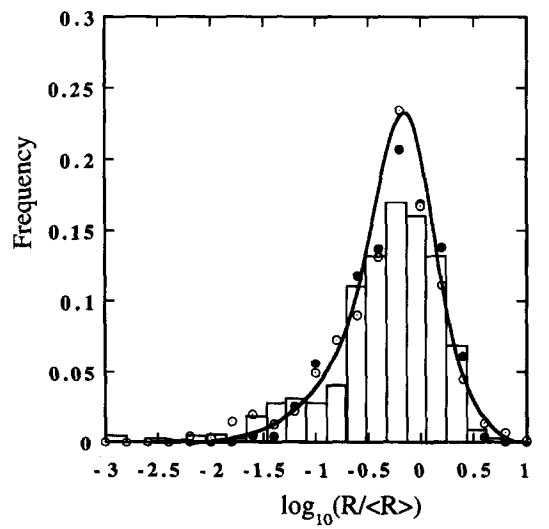

Fig. 18. Effect of volume fractions on grain size distributions in the system $R_\alpha = 1.4$, $R_\beta = 0.97$. The solid line is the distribution of the 90% α phase. Solid dots represent the distribution of the 10% β phase. The histogram is the initial distribution for both phases.

Acknowledgements—This work is supported by the National Science Foundation under grant number DMR 93-1898 and the simulations were performed at the Pittsburgh Supercomputing Center.

REFERENCES

1. French, J. D., Harmer, M. P., Chen, H. M. and Miller, G. A., *J. Am. Ceram. Soc.*, 1990, **73,** 2508.
2. Lange, F. F. and Hirlinger, M. M., *J. Am. Ceram. Soc.*, 1987, **70,** 827.
3. Alexander, K. B., Becher, P. F., Waters, S. B. and Bleier, A., *J. Am. Ceram. Soc.*, 1994, **77,** 939 and references therein.
4. Ankem, S. and Margolin, H., *Proc. 5th Int. Conf. on Titanium*, Vol. 3, Munich, 1984. Deutsche Gesellsschaft Fur Metallkunde E. V., F.R.G., p. 1705.
5. Grewa, G. and Ankem, S., *Metall. Trans. A*, 1989, **20,** 39–54.
6. Atkinson, H. V., *Acta metall.*, 1988, **36,** 469 and references therein.
7. Smith, C. S., *Trans. AIME*, 1948, **175,** 15.
8. Hilllert, M., *Acta metall.*, 1965, **13,** 227.
9. Louat, N. P., *Acta metall.*, 1974, **22,** 721.
10. Voorhees, P. W., *Ann. Rev. Mater. Sci.*, 1992, **22,** 197–215 and references therein.
11. Grewal, G. and Ankem, S., *Acta metall. mater.*, 1990, **38,** 1607.
12. Lifshitz, I. M. and Slyozov, V. V., *J. Phys. Chem. Solids*, 1961, **19,** 35.
13. Hillert, M., *Acta metall.*, 1988, **36,** 3177.
14. Srolovitz, D. J., Anderson, M. P., Grest, G. S. and Sahni, P. S., *Acta metall.*, 1984, **32,** 1429.
15. Doherty, R. D., Srolovitz, D. J., Rollett, A. D. and Anderson, M. P., *Scripta metall.*, 1987, **21,** 675.
16. Hassold, G. N., Holm, E. A. and Srolovitz, D. J., *Scripta metall.*, 1990, **24,** 101.
17. Cahn, J. W., *Acta metall. mater.*, 1991, **39,** 2189.
18. Holm, E. A., Srolovitz, D. J. and Cahn, J. W., *Acta metall. mater.*, 1993, **41,** 1119.
19. Cahn, J. W. and Van Vleck, E. S., *Scripta metall.*, submitted.
20. Cahn, J. W. and Hilliard, J. E., *J. Chem. Phys.*, 1958, **28,** 258.
21. Chen, L. Q. and Danan Fan, *J. Am. Ceram. Soc.*, 1996, **79,** 1163.
22. Chen, L. Q., *Scripta. metall. mater.*, 1995, **32,** 115.
23. Danan Fan and Chen, L. Q., *Acta mater.*, 1997, **45,** 611.
24. Danan Fan and Chen, L. Q., *Acta mater.*, 1997, **45,** 1115.
25. Chen, L. Q., Chengwei Geng and Yang, W., *Phys. Rev. B*, 1994, **50,** 15752.
26. Danan Fan and Chen, L. Q., *Phil. Mag. Lett.*, 1997, **75,** 187.
27. Allen, S. M. and Cahn, J. W., *Acta metall.*, 1979, **27,** 1085.
28. Cahn, J. W., *Acta metall.*, 1961, **9,** 795.
29. Alexander, K. B., Case study on sintering of ceramics. Paper presented at American Ceramic Society Annual Meeting, Cincinnati, OH, April 1995.